UV Observations with the *Transition Region and Coronal Explorer*

B. N. Handy (handy@physics.montana.edu)
Department of Physics
Montana State University – Bozeman
Bozeman, MT 59717

M. E. Bruner, T. D. Tarbell, A. M. Title and C. J. Wolfson
Lockheed-Martin Palo Alto Advanced Technology Center
Palo Alto, CA 94303

M. J. Laforge and J. J. Oliver
Acton Research Corporation
Acton, MA 01720

(Received: ......; Accepted: ......)

Abstract. The *Transition Region and Coronal Explorer* is a space-borne solar telescope featuring high spatial and temporal resolution. TRACE images emission from solar plasmas in three extreme-ultraviolet (EUV) wavelengths and several ultraviolet (UV) wavelengths, covering selected ion temperatures from 6000 K to 1 MK. The TRACE UV channel employs special optics to collect high resolution solar images of the H I Lα line at 1216 Å, the C IV resonance doublet at 1548 and 1550 Å, the UV continuum near 1550 Å and also a white light image covering the spectrum from 2000–8000 Å.

We present an analytical technique for creating photometrically accurate images of the C IV resonance lines from the data products collected by the TRACE UV channel. We use solar spectra from several space-borne instruments to represent a variety of solar conditions ranging from quiet sun to active regions to derive a method, using a linear combination of filtered UV images, to generate an image of solar C IV 1550 Å emission. Systematic and statistical error estimates are also presented. This work indicates that C IV measurements will be reliable for intensities greater than 10^{14} photons $\mathrm{s^{-1}cm^{-2}sr^{-1}}$. This suggests that C IV 1550 Å images will be feasible with statistical error below 20% in the magnetic network, bright points, active regions, flares and other features bright in C IV. Below this intensity the derived image is dominated by systematic error and read noise from the CCD.

Keywords: TRACE – solar transition region

1. Introduction

The ultraviolet (UV) spectrum provides a wealth of diagnostics for plasmas in the solar transition region and chromosphere. H I Lα 1216 Å and C IV 1550 Å (hereafter referred to as C IV) in particular are interesting lines for observing plasmas with temperatures from 10,000–100,000 K.

Ly α provides prominence images with considerable structure at the solar limb (Damé *et al.* 1996; Mariska and Withbroe 1975). Ly α images also bridge the gap between chromospheric visible light observations and more sparse observations in the transition region (Bonnet *et al.* 1980). Essentially all transition region models (see Fontenla *et al.* 1990 and references therein) have Ly α as the main energy loss mechanism below 10^5 K. C IV is an interesting diagnostic in a variety of ways. It has, for example, been suggested (Bruner & McWhirter 1988; Doyle 1996) that the total radiated power of an emitting plasma may be deduced from the intensity of C IV. Hawley & Fisher (1994) suggest that the C IV flux serves as a pressure diagnostic under appropriate conditions. Brekke *et al.* (1996) and Rottman *et al.* (1993) have observed C IV flare intensities to vary by a factor of $\approx 15,000$ over pre-flare levels.

However, C IV is a difficult line to observe. At 1550 Å, C IV sits atop a UV continuum background that increases five orders of magnitude in intensity over 1200–3500 Å. Various methods have been attempted to generate a “clean” C IV image. The *Ultraviolet Spectrometer and Polarimeter* on the *Solar Maximum Mission* was capable of collecting images by rastering a grating over a 256×256 pixel image with 3 arcsecond pixels (Woodgate *et al.* 1980). The *High Resolution Telescope and Spectrograph* (HRTS) employed a tandem Wadsworth Spectrograph with spatial resolution of 1 arcsecond along a 1000 arcsecond slit. HRTS was able to step the slit to cover a 10×800 arcsecond region in 20 seconds. Consequently HRTS was able to map a portion of the solar atmosphere as a function of time (Dere *et al.* 1984). The *Solar Ultraviolet Measurements of Emitted Radiation* (SUMER) experiment on the *Solar and Heliospheric Observatory* is a spectrograph capable of stepping across the solar disk to generate full-sun images with pixel sizes of ≈ 1 $arcsec\ px^{-1}$ and 20-40 $m\text{Å}\ px^{-1}$, again at the expense of temporal resolution (Wilhelm *et al.* 1995). The *Solar Plasma Diagnostic Experiment* rocket payload (SPDE, Damé *et al.* 1996) observed in C IV and neighboring wavelengths using multilayer optics in the *Transition Region Camera* (TRC, Bonnet *et al.* 1982, Foing *et al.* 1986). The design approach for the TRC was the catalyst for the TRACE UV channel.

The UV channel of TRACE was designed with the intent of estimating C IV emission on a strong UV background. The UV filters in TRACE were chosen to satisfy this requirement, and an analysis with sample solar spectra has been performed to illustrate this approach.

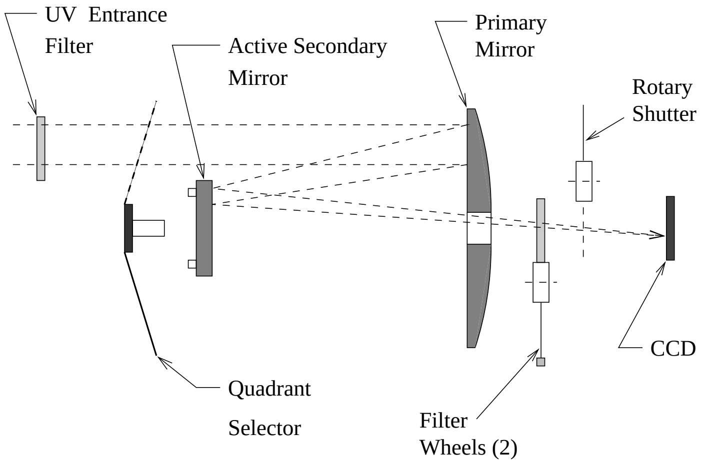

Figure 1. The TRACE Optical Path.

Table I. Telescope Characteristics.

Primary Mirror Diameter	30 cm
Effective Focal Length	8.66 m
Pixel Size	21×21 μm
	0.5×0.5 arcsec
CCD Size	1024×1024 pixels
Field of View	8.5×8.5 arcmin
Wavelength Channels:	171 Å, 195 Å, 284 Å
	1216 Å, 1550 Å, White Light
Image Stabilization	$\pm$ 0.1 arcsec

2. Instrument Description

2.1. Overall Description

The TRACE instrument is a 30 cm aperture Cassegrain telescope intended to observe solar plasmas from 6000 to 1MK with 1 arcsecond spatial resolution and high temporal resolution and continuity (Tarbell *et al.* 1994). The optical path of the telescope is illustrated in Figure 1 and the principal characteristics are given in Table I.

To provide wavelength discrimination the telescope is divided into four quadrants, each of which is sensitive to a different wavelength range. Three of these quadrants are sensitive in the extreme ultraviolet (EUV) and the fourth in the far UV through the visible wavelengths. The EUV quadrant bandpass selections are determined by multilayer coatings on the primary and secondary mirrors. The UV quadrant employs a narrowband all-dielectric primary mirror coated for wavelength selection and a secondary mirror coated with Al and MgF_2. Further wavelength discrimination is accomplished via a selection of broadband and narrowband filters (c.f. § 2.2). Visible light is excluded from the EUV quadrants by thin aluminum entrance filters mounted on a nickel mesh in front of each EUV quadrant. The UV quadrant is shielded by a broadband UV filter. A quadrant selector located directly behind the entrance filters selects which of the four channels is active. Two filter wheels, located aft of the primary mirror, provide further stray light rejection in the EUV and wavelength selection at the various UV wavelengths (discussed further in § 2.2). The filtered images are detected by a lumigen-coated CCD[1].

2.2. UV Performance

The UV channel of TRACE posed a restrictive set of requirements on the optics. One design goal was to be able to image both Ly α and C IV emission. A subsidiary goal was to acquire a useful image in the visible continuum at an exposure greater than $\sim$ 20 ms. Imaging at Ly α and C IV imposed the most difficulty on the design because this mandated a need for a broadband filter in the UV that would provide adequate transmission at both of the UV wavelengths while providing sufficient rejection at the longer wavelengths. It was necessary to balance transmission, rejection and bandpass to optimize 1216 Å and 1550 Å throughput. All UV coatings were designed and manufactured by Acton Research Corporation (Acton, MA).

The resultant entrance window filter is a single crystal 118 mm dia.$\times$10 mm thick MgF_2 substrate coated with a broadband multilayer metal-dielectric interference coating. The coating was optimized to transmit about equally at 1216 Å and 1550 Å while simultaneously providing good rejection at the visible wavelengths.

The primary and secondary mirror coatings are a compromise between reflecting Ly α and C IV and rejecting visible light. The primary mirror is coated with an all-dielectric multilayer interference coating with peak reflection of approximately 83% at 1540 Å and a bandwidth of 150 Å FWHM. The reflectivity drops to 10% at 1216 Å and at wavelengths above 1600 Å. The primary is designed to enhance the signal-to-noise ratio for C IV by rejecting long-wavelength light. This coating has the beneficial effect of reducing the heat load and UV flux on the secondary mirror. The UV quadrant of the secondary mirror is

[1] Substantial confusion exists on the spelling of "lumigen". It is referred to in the literature as lumigen, liumogen and lumogen. All refer to the same material.

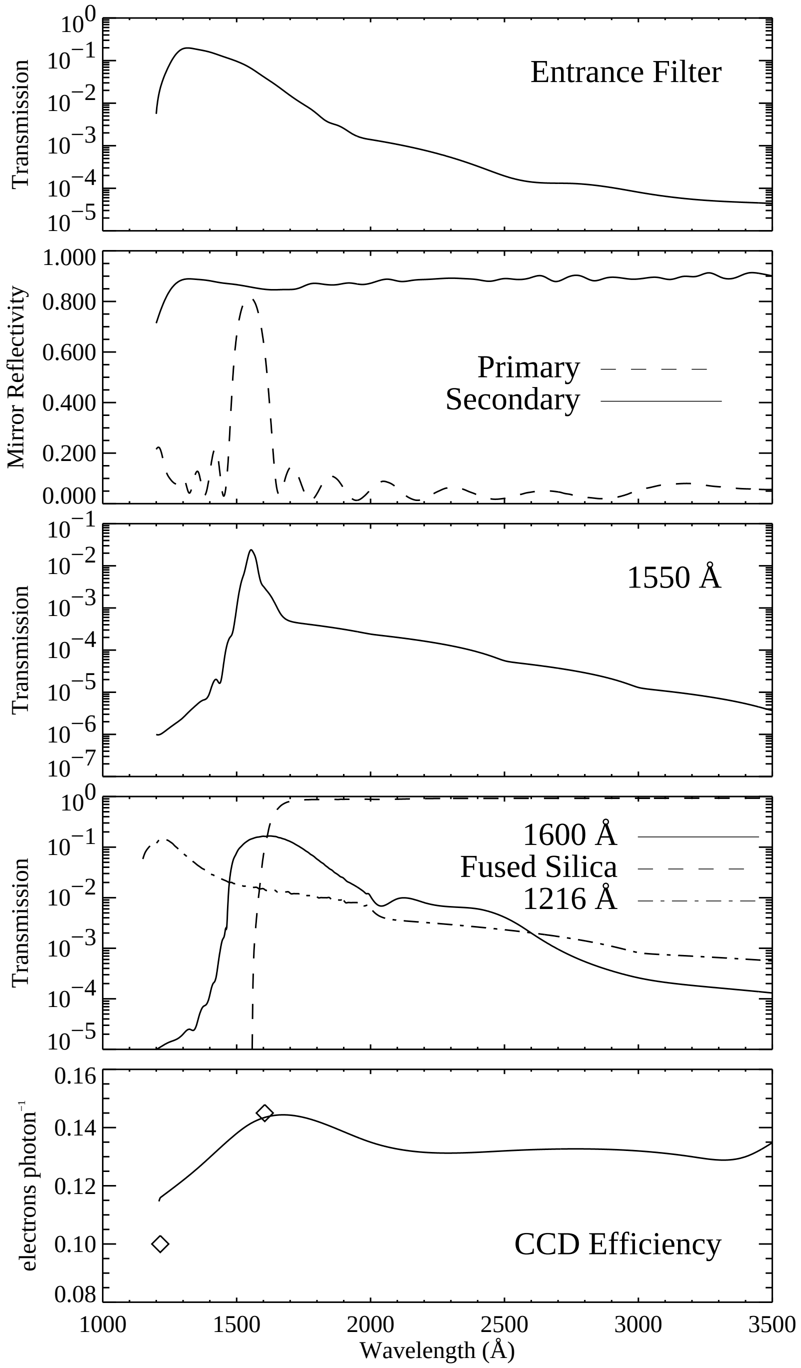

Figure 2. UV response of the individual UV optical components of TRACE. The data points in the bottom graph at 1215 and 1605 Å show measured efficiency of witness samples Lumigen-coated with the TRACE CCD. See text.

Table II. TRACE Filter Properties

Solar Emission	Substrate	Central Wavelength	FWHM	Peak Transmission
Carbon IV	CaF_2	1550 Å	37 Å	2.4%
Ly α	MgF_2	1216 Å	80 Å	14.1%
UV Continuum	Crystalline Quartz	1600 Å	245 Å	16.6%
White Light	Fused Silica	N/A	N/A	94%

coated with aluminum and a thin film MgF_2 overcoating to prevent oxidation and optimize the coating for 1550 Å.

The filter wheels contain the UV filters described in table II. The filters of interest for this problem are the 1550 Å filter, the 1600 Å filter and the fused silica filter. In figure 2 we show the transmission curves for these filters. The 1550 Å filter is particularly noteworthy as it is an induced transmission filter (Macleod 1986). Extra-narrowband filters with this bandpass typically suffer from sidebands which contaminate the desired emission line; the filter flying in TRACE does not. This filter has a FWHM of 37 Å and long-wavelength rejection of order 10^{-6}. The 1600 Å filter is a narrowband filter with FWHM of 245 Å and will be used in tandem with the fused silica filter to evaluate the long-wavelength continuum. Substrate thickness for each of the UV filters was specified in an attempt to minimize change in focus when switching between wavelengths.

The TRACE CCD (three-phase, multi-pinned phase, unthinned, front-illuminated) is almost identical to the detector used in the Michelson Doppler Imager on SoHO (MDI, Scherrer *et al.* 1995) and is in fact an MDI flight spare made by Loral Aerospace Corporation. The front surface is coated with lumigen. Lumigen is a fluorescent coating that sensitizes the CCD to UV and EUV wavelengths (Deeg *et al.* 1994; Kristianpoller *et al.* 1964). The quantum efficiency (QE) measurements used in this analysis are taken from the Ford/CRAF Cassini CCD (Janesick 1994) as the TRACE CCD is similar to that device. The broadband coverage provided by the above measurement makes the analysis in this paper possible. Slides coated with the TRACE CCD have been measured at 1215 Å and 1605 Å (c.f. the bottom curve in figure 2). The TRACE CCD is $\approx$ 12% lower in quantum efficiency at Ly α and nominally the same at 1605 Å. The photodiodes used for this calibration have a 10% absolute uncertainty in quantum efficiency. Since the 1215 Å result has little effect on TRACE C IV analysis, the Cassini measurements were used verbatim for the calculation that follows.

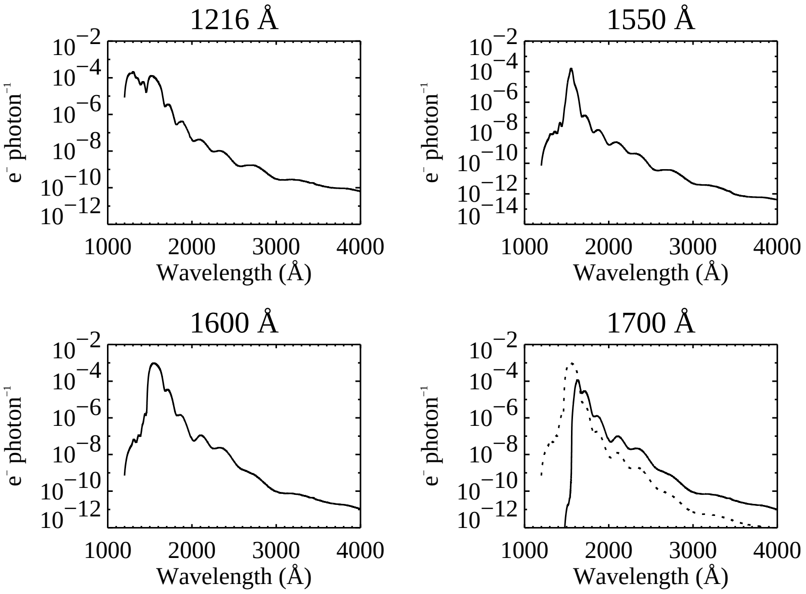

Figure 3. Spectral response of the UV channel. The 1700 Å image is composed of an image with the 1600 Å filter in series with a fused silica substrate. The dotted curve in the lower right-hand graph represents a "clean 1600 Å" curve given by the difference between the 1600 Å and scaled 1700 Å images as described in equation 4.

3. Analysis

3.1. Photometry and Analysis

The optical response of the UV quadrant may be represented by the relation

$$I(\lambda, t) = F(\lambda, t)T(\lambda)Q(\lambda)\Omega A \tag{1}$$

where $I(\lambda, t)$ represents the number of electrons pixel^{-1} Å^{-1} s^{-1} generated at the CCD, $F(\lambda, t)$ represents the solar flux with units of photons s^{-1} Å^{-1} cm^{-2} sr^{-1}, $T(\lambda)$ represents the combined optical response of the mirrors and analysis filters, $Q(\lambda)$ represents the quantum efficiency of the detector (electrons photon^{-1}), Ω represents the solid angle subtended by one pixel (0.5×0.5 arcsec or $\approx 5.876 \times 10^{-12}$ sr) and A represents the clear aperture of the UV quadrant (91.0 cm^2). Note that the CCD doesn't actually yield a solar spectrum but yields a detection rate integrated over all wavelengths: $I(t) = \int_\lambda F(\lambda, t)T(\lambda)Q(\lambda)\Omega A d\lambda$.

A complete C IV dataset is composed of three images:

$$\begin{aligned} I_1 &= 1550 \text{ Å Image} \\ I_2 &= 1600 \text{ Å Image} \end{aligned} \tag{2}$$

$$I_3 \quad = \quad 1700 \text{ Å Image} = 1600 \text{ Å+Fused Silica Filters}$$

The quantity $[T(\lambda)Q(\lambda)\Omega A]$ in equation 1 describes the response function of the instrument. This quantity can then be calculated to yield response curves at the various wavelengths of interest. Response function curves for the Ly α channel and images I_1, I_2 and I_3 are given in Figure 3. The Ly α channel has a double peak at 1216 and 1550 Å. This is a result of the transmission of the Ly α filter coating and the coating on the primary, which is centered at 1550 Å. The 1700 Å image is a product of the 1600 Å filter in series with the fused silica substrate. The purpose of this combination is to measure the contribution from long-wavelength contamination.

Given the above three measurements, it should be possible to estimate three portions of the solar spectrum:

$$\begin{aligned} I_{\mathrm{C\ IV}} &= \text{1550 Å Intensity} \\ I_{\mathrm{CTN}} &= \text{Ultraviolet Continuum} \\ I_{\mathrm{WL}} &= \text{White-light Continuum} \end{aligned} \tag{3}$$

The goal of this exercise is to generate these three quantities from equations (2). This is done via a least-squares analysis with sample spectra from the HRTS mission, detailed in § 4.2. As a first step, however, it is useful to apply some physical intuition to the problem to eliminate one variable. The latter two images in (2) may be combined to generate a single "clean" narrowband UV continuum image near 1550 Å with a FWHM of ≈ 200 Å via the relation:

$$I_{2C} = I_2 - (1.07)I_3. \tag{4}$$

Each of the two resulting images (I_1 and I_{2C}) may be resolved into a linear combination of contributions from C IV and the UV continuum. This method suggests the following relationship:

$$\begin{aligned} I_{CIV} &= \alpha I_1 + \beta I_{2C} + \epsilon_{CIV} \\ I_{CTN} &= \gamma I_1 + \delta I_{2C} + \epsilon_{CTN}, \end{aligned} \tag{5}$$

where α, β, δ and γ are constants and ϵ_n represents the systematic error in this measurement. I_{CIV} and I_{CTN} represent the contributions from the C IV and UV continuum emission, respectively. The statistical error for this calculation is derived in § 3.2.

The TRACE response for a nominal active region spectrum is illustrated in figure 4.

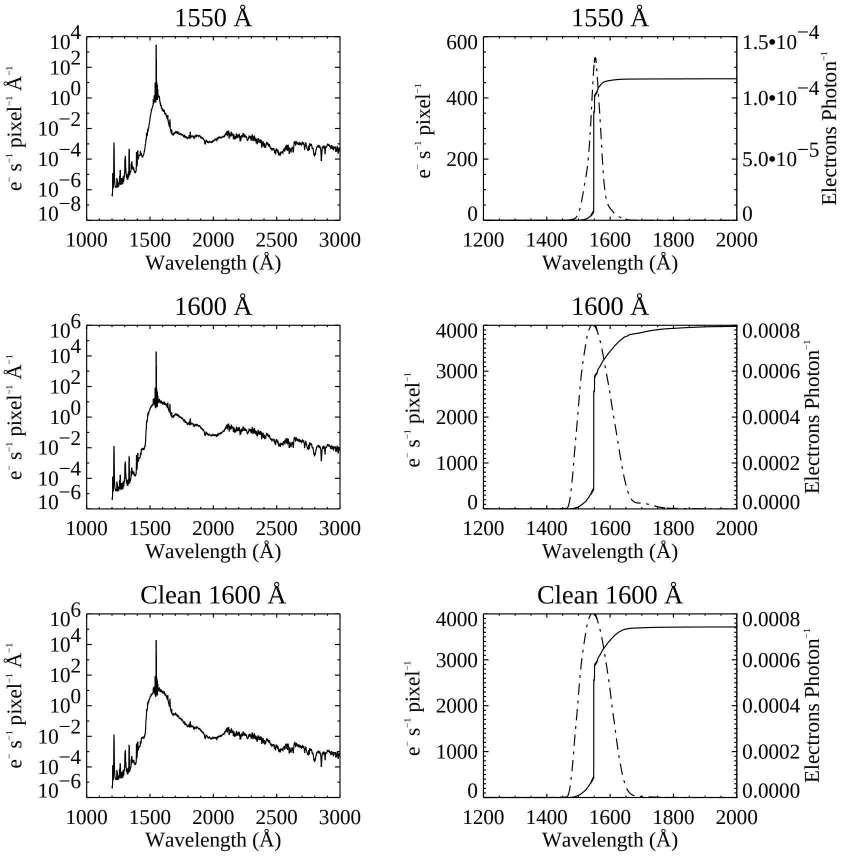

Figure 4. TRACE instrument response to an active region solar spectrum. The "Clean 1600 Å" spectra is a difference of the 1600 and scaled 1700 Å spectra. The plots at right indicate (solid line) the running integral contribution to the CCD signal, and (dotted line) the instrument throughput.

3.2. Error Propagation

In the previous section we constructed a set of equations to calculate the intensity in C IV and the UV continuum at 1550 Å. In this section we derive the statistical error in the data due to Poisson counting statistics.

For the three images of equation 2, the error due to photon statistics and read noise in the CCD is given by

$$s_n = \sqrt{\frac{I_n}{t_n} + \left(\frac{RN}{t_n}\right)^2} \tag{6}$$

In (6), I_n represents the intensity of a pixel in each respective image, s_n represents the standard deviation of the corresponding photon detection rate, t_n represents the exposure time and RN is the read noise of the CCD ($\approx$ 20 electrons).

In equation 4 we derived a 1600 Å continuum image bereft of visible contamination, and the corresponding error is given by

$$s_{2C} = \sqrt{s_2^2 + (1.07)^2 s_3^2} \tag{7}$$

where the factor of 1.07 is the scaling factor due to the fused silica substrate. It then follows that the uncertainty in the calculated C IV and continuum levels is given by

$$\begin{aligned} s_{CIV} &= \sqrt{\alpha^2 s_1^2 + \beta^2 s_{2C}^2} \\ s_{CTN} &= \sqrt{\gamma^2 s_1^2 + \delta^2 s_{2C}^2} \end{aligned} \tag{8}$$

At this point, we've mentioned two forms of error: the systematic error in the calculation contained in ϵ, which is the absolute error in the calculation for a given solar spectrum, and the error due to photon statistics contained in s_n. In § 4.2 we present results of both types of error for the dataset used in this paper, calculated as a fractional error – the ratio of the error to the desired answer. In this guise, a fractional error of 1.0 indicates the uncertainty is equal to the desired answer. It is possible that the systematic error may be improved upon through new techniques and on-orbit calibrations, but the standard deviation is unlikely to change significantly. Improvements to the standard deviation will only be seen in significantly longer exposure times or brighter sun.

4. C IV Estimates

4.1. Spectral Data

To predict the results for TRACE we compiled a set of solar spectra to fold through the optical response function. UV data are only available from spaceborne instruments, and no single instrument has been able to collect data over the large spectral range we are interested in: ≈1200–10000 Å. It was therefore necessary to obtain data from several sources and merge the spectra together (see figure 5).

The SOLSTICE instrument (Rottman *et al.* 1993) is a rich source of irradiance spectra but is limited in that the spectral resolution is only 1.5 Å and it provides only a full-disk average intensity. This dataset provided a useful spectral baseline and covered the spectral range 1200–4000 Å. To provide for better spectral resolution and to also reflect solar

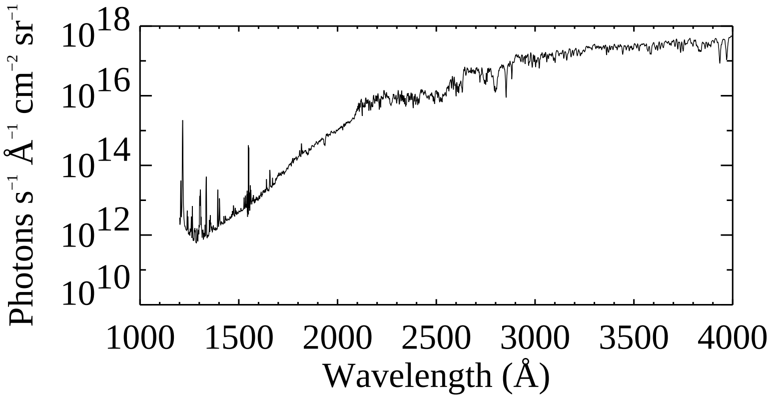

Figure 5. Representative network solar spectrum from SOLSTICE and HRTS.

variability from quiet sun to active regions, we employed HRTS data over the 1540–1559 Å range (Brekke *et al.* 1993, 1994, 1995). To fill out the visible and infrared spectrum to the upper limit of the CCD response (1 μm) we employed radiance spectra from Pierce & Allen (1977). We are combining radiance (a measurement of the intensity at the source) and irradiance (the intensity as measured at 1 AU) data in this model. While this is not a completely accurate method of creating a sample solar spectrum, it is sufficient for our purposes. The solar spectrum is accurate within the bandpass of the instrument (1400-1800 Å), and the approximated spectrum above and below this region only provides a minor contribution to the image.

The HRTS data (Brekke 1995) provide a comprehensive set of stigmatic spectra over the range 1540–1559 Å across a large extent of the solar disk from near sun center to the solar limb. Each spectral trace in this dataset was in turn matched to the SOLSTICE data. For $\lambda < 1540$ Å SOLSTICE was scaled by a constant to match continuum levels of the HRTS data. For 1559 Å $< \lambda <$ 2100 Å, the SOLSTICE spectra was scaled by a function matching the continuum at 1559 Å. The scaling function was constrained to be unity at 2100 Å, where the variability of the solar disk is lower and the throughput of the TRACE instrument is down by several orders of magnitude.

4.2. Results

In order to solve for the coefficients in eqn. 5 it is necessary to define *a priori* what I_{CIV} and I_{CTN} represent. For this study I_{CIV} represents the emission from the C IV doublet at 1548 and 1550 Å with the

UV background removed, and I_{CTN} represents the UV continuum and other emission lines in the range 1540–1559 Å. The continuum definition is somewhat arbitrary but represents the UV filters in TRACE reasonably well. The UV response of the system was then convolved with the merged HRTS/SOLSTICE spectra to predict the TRACE response to a variety of solar C IV and UV continuum emission features. We then calculated the actual emission, compared it to the observed intensities in each of the filter combinations and generated the set of solutions to equations 5 via a least-squares analysis:

$$\begin{pmatrix} \alpha & \beta \\ \gamma & \delta \end{pmatrix} = \begin{pmatrix} 1.55 \times 10^{13} & -1.09 \times 10^{12} \\ -3.10 \times 10^{12} & 4.94 \times 10^{11} \end{pmatrix}. \tag{9}$$

Given the above coefficients, it is possible to make empirical estimates of the measurement errors. The following calculations were generated with exposure times of 10 seconds for 1550 Å, 2 seconds for 1600 Å and 5 seconds for 1700 Å. There are two sources of error to consider. The first and easier to quantify is that due to Poisson statistics and read noise in the TRACE CCD, illustrated in figure 6 and § 3.2. Below a C IV intensity of $\approx 10^{14}$ photons $\mathrm{s}^{-1}\mathrm{cm}^{-2}\mathrm{sr}^{-1}$ the signal is dominated by the read noise of the CCD. This threshold intensity suggests we will be able to calculate useful numbers for bright network, active regions, flares and other relatively bright features. Somewhat fainter features will be measureable only with significantly longer exposure times.

It is also useful to examine the systematic error that is a result of this method of calculation; this is the term ϵ_{CIV} in equation 5, assuming no noise in the measured intensities. These results are presented in figure 7. They do not quite reflect reality as the variability of the emission lines outside 1540–1559 Å contaminating the C IV image was not considered in this exercise. The narrow bandwidth of the filters however should serve to minimize this effect. Based on these results we can expect a systematic error of less than 20% for bright features.

It is interesting to generate a linear combination of the 1550 Å, 1600 Å and 1700 Å filters as suggested by equations 5. This results in a set of "effective filters" for C IV and the UV continuum emission illustrated in figure 8. The graphs are a pleasing visual check of the C IV and continuum extraction techniques. The C IV "filter" is heavily weighted towards the C IV emission line, while the resulting UV continuum "filter" attempts to isolate the continuum around 1550 Å while rejecting C IV. The negative transmission present in the C IV curve is in effect a method of measuring the mean intensity for the underlying UV continuum at 1550 Å.

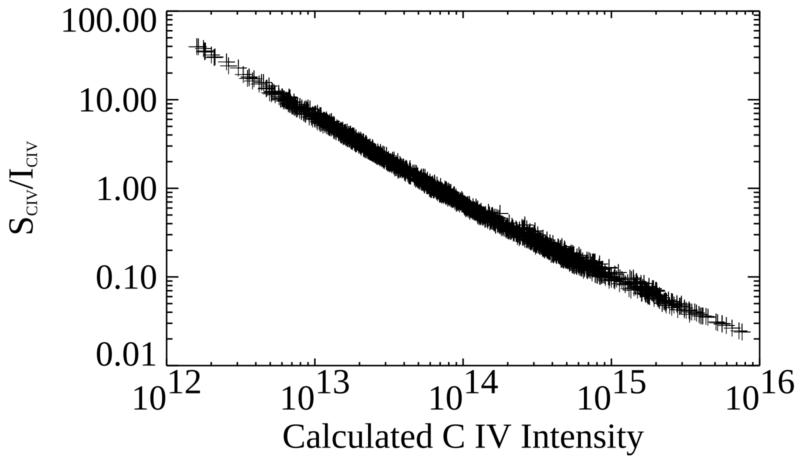

Figure 6. Fractional standard deviation of the calculated C IV intensity based on Poisson counting statistics and a CCD read noise of 20 electrons. Below a C IV intensity of $\approx 10^{14}$ photons $s^{-1}cm^{-2}sr^{-1}$ the noise is dominated by CCD read noise. Standard deviation is based upon a 10 second 1550 Å exposure, a 2 second 1600 Å exposure and a 5 second 1600 Å+fused silica exposure.

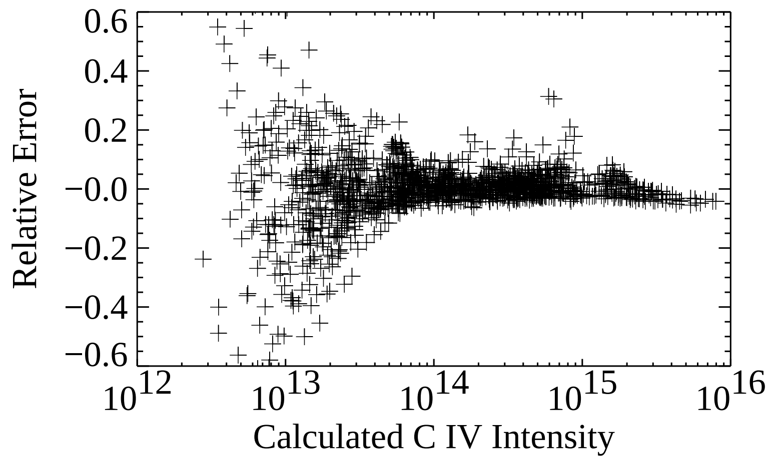

Figure 7. Relative systematic error ($\epsilon_{\rm CIV}/I_{\rm CIV}$) observed in calculating C IV intensity from the HRTS data. Intensity is in units of photons $s^{-1}cm^{-2}sr^{-1}$.

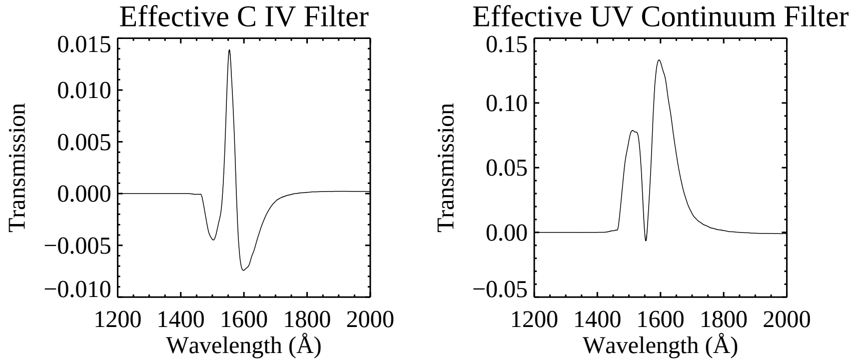

Figure 8. Effective Transmission of the TRACE C IV and UV continuum channels. These curves represent a linear combination of the 1550 Å, 1600 Å and 1700 Å response functions. The effective C IV filter isolates the 1550 Å lines, while the continuum filter rejects these lines.

5. Discussion

We have presented a method of estimating C IV 1550 Å emission from the UV dataset that will be collected by the TRACE instrument. Data from the SOLSTICE and HRTS missions were combined with ground-based data to generate a large set of synthetic solar spectra to model TRACE performance. Coefficients were generated via a least-squares fit to generate a set of linear equations for estimating the true C IV and UV continuum levels from the TRACE UV dataset. The data were then folded back through this system to generate Poisson statistics and an analysis of the systematic (e.g. relative) error in this system. Our analysis suggests that the best results will be achieved in regions of C IV 1550 Å intensity greater than $\approx 10^{14}$ photons $s^{-1}cm^{-2}sr^{-1}$. Below this intensity the calculation becomes overwhelmed by CCD read noise, counting statistics and the simple nature of the simple model used in this analysis. It is possible to imagine a more advanced model that varies with intensity and solar conditions, but this quickly becomes both difficult and error-prone notion. For each pixel, there are only three measurements available from the different filter combinations. This small quantity of information is not sufficient to support a dramatically more complex algorithm.

The manner in which the UV channel has been designed allows for some flexibility in formulating observing sequences. The Ly α channel will be of particular interest near the beginning of the mission, as it will provide an opportunity to observe this wavelength with high temporal cadence for an extended period of time. It will be important to utilize this capability early in the mission, as it should be assumed there will be degradation in Ly α response due to contamination and radiation damage to the lumigen coating on the CCD. To aquire C IV 1550 Å data, the method as suggested in this paper is to always collect a triplet of exposures in 1550, 1600 and 1700 Å. A typical cadence for such an exposure set would be on the order of 30 seconds.

There is some evidence that suggests the brightest features in the C IV lines will also be evolving the most rapidly, and thus critical data in the evolution of these features may pass unobserved. There are several ways of approaching this problem. One method would be to only collect occasional images in the UV continuum at 1600 Å and 1700 Å and then a rapid sequence of 1550 Å images, using the first pair of background images to correct each frame for C IV emission. Another technique that may be considered is to merely take a rapid sequence of images through the 1600 Å filter. This image will contain a large UV continuum background component, but the brightest and most rapidly varying features will likely be emitting in the C IV resonance lines. This may provide a technique to see C IV "blinkers".

Lastly, the fused silica filter will be used to generate short exposure ($\approx$ 20 msec) white light images with a cadence of a few seconds. These images will contain almost equal contributions over the spectral range 2000–8000 Å.

With added experience and on-orbit calibration, refinements to the model presented here is expected. It is anticipated that the SUMER experiment will be able to participate in limited coordinated observations during the early TRACE mission. It is also possible that some coordinated calibration work may be done with various full-sun UV irradiance experiments, e.g. SOLSTICE and the Solar Ultraviolet Spectral Irradiance Monitor (Lean *et al.* 1992).

6. Acknowledgments

This work was supported by contract NAS5-38099 with NASA Goddard Spaceflight Center. We are indebted to P. Brekke and the HRTS team for providing the data that made this analysis possible, and L. Shing who performed the Lumigen calibration on TRACE witness samples. We also thank L. W. Acton for critical comments on this work. BH is grateful for accomodation as a graduate study scientist with the Lockheed Martin Solar and Astrophysics Group during the preparation of the TRACE instrument and this paper.

References

Bonnet, R. M., Bruner, E. C., Acton, L. W., Brown, W. A., and Decaudin, M. 1980, *Astrophys. J.* **237**, L47.

Bonnet, R. M., Decaudin, M., Foing, B., Bruner, M., Acton, L. W., Brown, W. A. 1982, *Astron. Astrophys.* **111**, 125.

Brekke, P. 1993, *Astrophys. J. Suppl.* **87**, 443.

Brekke, P. and Kjeldseth-Moe, O. 1994, *Astrophys. J.* **431**, L55.

Brekke, P. 1995, Private Communication.

Brekke, P., Rottman, G. J., Fontenla, J. and Judge, P. G. 1996, *Astrophys. J.* **468**, 418.

Bruner, M. E. and McWhirter, R. W. P., 1988, *Astrophys. J.* **326**, 1002.

Damé, L., *et al.* 1996, *Adv. Space Res.* **17** (4/5), 189.

Deeg, H.-J. and Ninkov, Z. 1995, *Op. Eng.* **34**, 43.

Dere, K. P., Bartoe, J.-D. F. and Bruekner, G. E. 1983, *Astrophys. J.* **281**, 870.

Doyle, J. G. 1996, *Astron. Astrophys.* **307**, 162.

Foing, B., Bonnet, R.-M., and Bruner, M. 1986, *Astron. Astrophys.* **162**, 292.

Fontenla, J. M., Avrett, E. H. and Loeser, R. 1990, *Astrophys. J.* **355**, 322.

Hawley, S. L. and Fisher, G. H. 1994, *Astrophys. J.* **426**, 387.

Janesick, J., Jet Propulsion Laboratory 1994, private communication.

Kristianpoller, N. and Dutton, D. 1964, *Appl. Opt.* **3**, 287.

Lean., J., Vanhoosier, M. E. and Brueckner, G. 1992, *Geophys. Res. Letters* **19**, 2203.

Macleod, H. A. 1986, *Thin-Film Optical Filters*, Macmillan Publishing Co., 295.

Mariska, J. T. and Withbroe, G. L. 1975, *Solar. Phys.* **44**, 55.

Pierce, A. K., Allen, R. G. 1977, in *The Solar Output and its Variation*, ed. O. R. White, Colorado University Press, 169.

Rottman, G. J., Woods, T. N. and Sparn, T. P. 1993, *J. Geophys. Res.* **98**, 10667.

Scherrer *et al.* 1995, *Solar Phys.* **162**, 129.

Tarbell, T. D., *et al.* 1994, in *Proc. of the Third SoHO Workshop – Solar Dynamic Phenomena and Solar Wind Consequences*, 26-29 September 1994.

Wilhelm, K., *et al.* 1995, *Solar Phys.* **162**, 189.

Woodgate, B. E. *et al.* 1980, *Solar Phys.* **65**, 73.

Address for Offprints: Brian Handy
Department of Physics
Montana State University – Bozeman
P.O. Box 173840
Bozeman, MT 59717-3840